

Stimulated Forward Brillouin Scattering in Subwavelength Silicon Membranes

Paula Nuño Ruano^{1,*}, Jianhao Zhang², David González-Andrade¹, Daniele Melati¹, Eric Cassan¹, Pavel Cheben², Laurent Vivien¹, Norberto Daniel Lanzillotti-Kimura¹, and Carlos Alonso-Ramos¹

¹*Centre de Nanosciences et de Nanotechnologies, CNRS, Université Paris-Saclay, Palaiseau 91120, France*

²*National Research Council Canada, 1200 Montreal Road, Bldg. M50, Ottawa, Ontario K1A 0R6, Canada*

**Corresponding author: paula.nuno-ruano@c2n.upsaclay.fr*

Abstract

On-chip Brillouin scattering plays a key role in numerous applications in the domain of signal processing and microwave photonics due to the coherent bidirectional coupling between near-infrared optical signals and GHz mechanical modes, which enables selective amplification and attenuation with remarkably narrow linewidths, in the kHz to MHz range. Subwavelength periodic nanostructures provide precise control of the propagation of light and sound in silicon photonic circuits, key to maximize the efficiency of Brillouin interactions. Here, we propose and demonstrate a new subwavelength waveguide geometry allowing independent control of optical and mechanical modes. Two silicon lattices are combined, one with a subwavelength period for the light and one with a total bandgap for the sound, to confine optical and mechanical modes, respectively. Based on this approach, we experimentally demonstrate optomechanical coupling between near-infrared optical modes and GHz mechanical modes with 5-8 MHz linewidth and a coupling strength of $G_B = 1360 \text{ W}^{-1} \text{ m}^{-1}$. A Stokes gain of 1.5 dB, and anti-Stokes loss of -2 dB are observed for a 6 mm-long waveguide with 35.5 mW of input power. We show tuning of the mechanical frequency between 5 and 8 GHz by geometrical optimization, without loss of the optomechanical coupling strength.

Key words: Brillouin Scattering, Subwavelength, Silicon Photonics

1 Introduction

Brillouin scattering (BS) refers to the inelastic scattering of light by acoustic phonons. The stimulated regime (SBS) yields the strongest third-order optical nonlinearity for many dielectric materials. Currently, Brillouin scattering is being exploited in optical fibers and integrated

devices to implement a wide range of devices, including ultra-narrow linewidth lasers [1], radio-frequency (RF) signal generators [2] and filters [3], distributed sensors [4], optical storage [5], and quantum applications [6].

Historically, research on SBS was led by the optical fiber community, [7], and more recently, on-chip optomechanical micro- and nano-structures have attracted great interest for their ability to enhance and tailor these interactions through a combination of electrostriction and radiation pressure forces [8]. Among the many integrated platforms developed in the last decade to harness BS [9], silicon-based devices have experienced noteworthy progress since the first experimental observation in 2013 [10] due to the strong optomechanical interactions and compatibility with standard CMOS technology.

Silicon-on-insulator (SOI) platform faces an important challenge: the simultaneous confinement of optical and mechanical modes within the waveguide. The strong phonon leakage towards the silica under-cladding [9] hinders efficient Brillouin interactions in SOI geometries. Suspended or quasi-suspended structures such as membrane rib waveguides [11], fully suspended nanowires [12], and pedestal waveguides [13] have proven to be an efficient solution towards achieving large Brillouin gain through forward stimulated BS (FSBS). However, these structures show a reduced fabrication tolerance or poor mechanical stability or rely on extremely low optical loss to compensate for a moderate Brillouin gain. Subwavelength silicon waveguides [14] emerge in this context as an alternative for more stable designs with comparable or improved optomechanical interactions. Moreover, FSBS couples longitudinally propagating photons and transversally propagating phonons [9]. Hence, subwavelength engineering of the longitudinal and transversal geometries allows independent control of photonic and phononic modes.

Here, we propose a suspended waveguide design that exploits a single-etch subwavelength structure to facilitate fabrication and mechanical stability combined with a phononic crystal to provide mechanical confinement. This geometry yields a significant Brillouin gain of up to 1.5 dB of Stokes gain in a 6 mm-long waveguide with 35.5 mW of input power. Additionally, we show the tunability of the SBS resonant frequency by varying the lengths of the subwavelength arms and the waveguide width without detriment of the performance.

2 Design and Simulation

The optomechanical waveguide, depicted in **Figure 1**, comprises a suspended central core shielded from the lateral silicon slabs by a cladding comprising a lattice of silicon arms and a phononic crystal barrier. The inner part of the cladding ensures propagation in the sub-wavelength regime for the fundamental transverse electric (TE) optical mode and separates the phononic crystal from the optical mode, hence allowing for reduced optical propagation losses. The outermost part of the cladding consists of phononic crystal with an air cross as a unit cell along a square lattice [15], and it is designed to confine a set of mechanical modes by Bragg reflections within the waveguide core and inner cladding. A single thickness is considered for the whole waveguide, allowing fabrication in a single-etch step.

We restrict ourselves to the intramodal forward Brillouin scattering (FBS), which is known to provide the most efficient optomechanical interactions in integrated silicon nanostructures. Intramodal FBS is a three-wave process that involves two copropagating optical photons, pump and signal, guided in the same optical spatial mode, and a phonon that mediates the interaction between them. This coupling must satisfy the energy conservation $\omega_s = \omega_p \pm \Omega$ and the phase-matching condition $q(\Omega) = k(\omega_p) - k(\omega_s)$, where $k(\omega)$ is the optical wavevector at

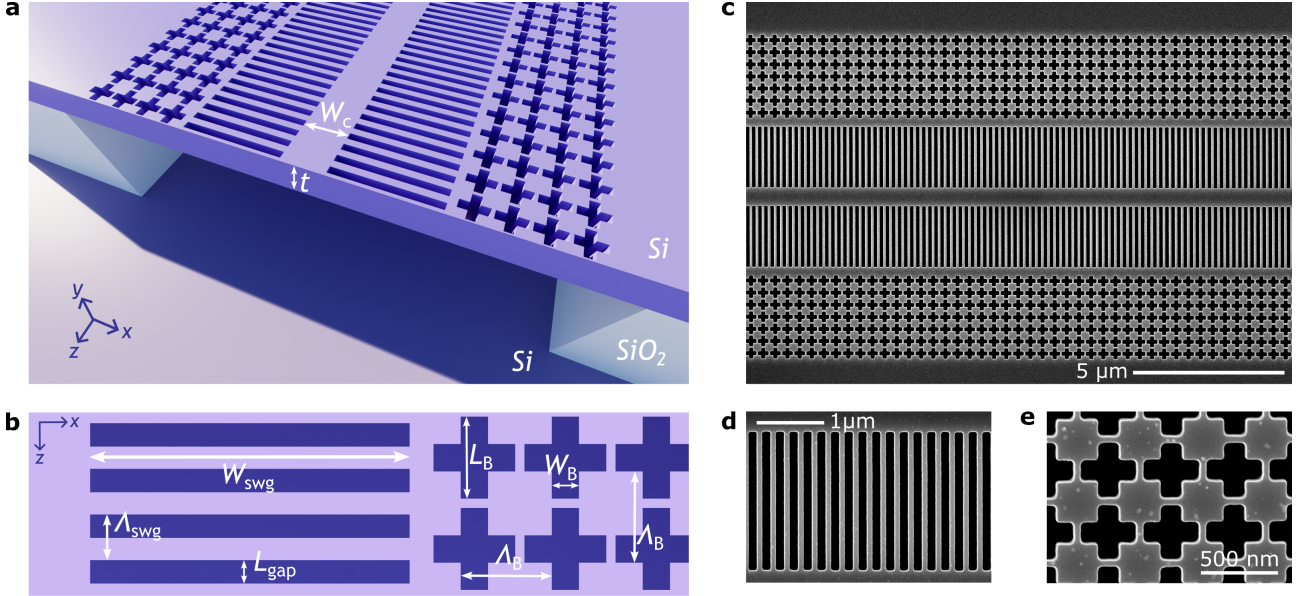


Figure 1: Proposed optomechanical waveguide. a) – b) Schematic view of the proposed design, with the definition of the geometrical parameters. c) – e) SEM images of the fabricated waveguide with parameters $W_c = 600$ nm, $t = 220$ nm, $\Lambda_{\text{swg}} = 200$ nm, $L_{\text{gap}} = 120$ nm, $W_{\text{swg}} = 2$ μm , $L_B = 350$ nm, $W_B = 140$ nm, and $\Lambda_B = 400$ nm.

optical frequency ω and $q(\Omega)$, the acoustic wavevector at mechanical frequency Ω . When the optical dispersion is negligible, as in subwavelength waveguides, the phase-matching condition is reduced to $q(\Omega) \approx 0$, and the same acoustic mode can effectively mediate the Stokes and anti-Stokes processes. Thus, intramodal FBS can enable cascaded light scattering and produce multiple optical sidebands [16].

The device (Figure 1) is fabricated from a standard (100) SOI wafer microchip with a top silicon layer of thickness $t = 220$ nm. The pattern is drawn using electron-beam lithography and dry etching and the buried oxide layer was removed using HF acid vapor. The optomechanical waveguide is aligned with the $\langle 110 \rangle$ direction of crystalline silicon and it has a total length of 6 mm and a central core width of $W_c = 600$ nm. The anchoring silicon arms are placed with a periodicity of $\Lambda_{\text{swg}} = 200$ nm and separated by a gap of $L_{\text{gap}} = 120$ nm. They have a width of $W_{\text{swg}} = 2$ μm , which isolates the optical mode from the phononic crystal. The latter consists of an air-cross unit cell of dimensions $L_B = 350$ nm and $W_B = 140$ nm placed along a square lattice of constant $\Lambda_B = 400$ nm. This geometry exhibits a large full bandgap between 5 and 8 GHz, as shown in **Figure 2a**. This structure guides the fundamental TE optical mode, which couples efficiently with the breathing modes of the waveguide core. The acoustic modes extend to the full width of the cavity formed by the phononic crystal slabs. Hence, our waveguide can support different transverse mechanical modes that yield good optomechanical interactions. In Figure 2b and 2c we illustrate the simulated TE optical mode at 1550 nm wavelength and mechanical displacement for the breathing mode.

3 Experimental Results

As previously mentioned, FBS in low-dispersive waveguides couples the Stokes and anti-Stokes processes. Thus, noise-initiated Brillouin interactions are very inefficient [17] and a stimulated

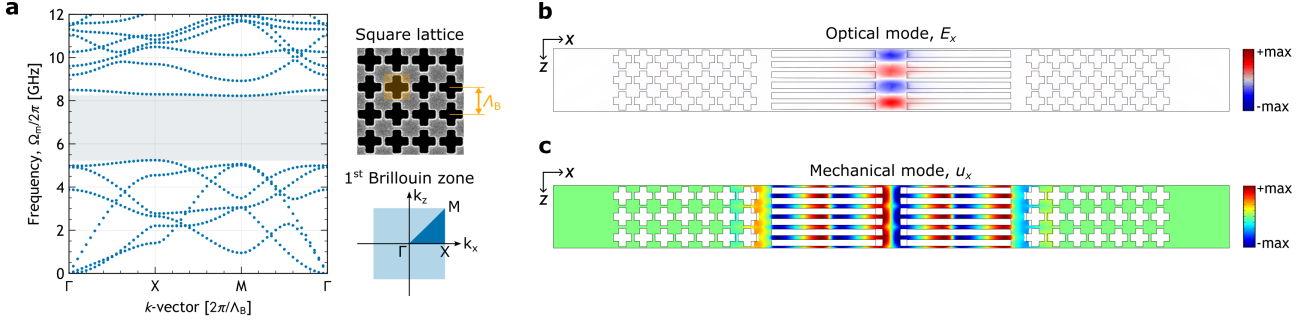


Figure 2: Optomechanical simulations. a) Phononic band structure, with a bandgap between 5 and 8 GHz. b) Simulated TE optical mode (E_x component) at 1550 nm wavelength. c) Simulated breathing mechanical mode (u_x displacement) at a frequency of 7.184 GHz.

process is required to obtain measurable Brillouin gain.

The standard stimulated FBS experiment [11, 12, 13] consists of inputting a pump and a Stokes signal in the waveguide and recording the Stokes gain as a function of the frequency separation between both lines. Generally, the Stokes line is obtained by modulation of the pump wave and hence, this configuration requires very narrow filters to remove the anti-Stokes sideband. In the absence of such performing filters, we choose to characterize the optomechanical response using a three-tone gain experiment [18], as illustrated in **Figure 3**. Here, we use a narrow-linewidth laser source at 1550 nm wavelength as the pump, which is modulated with an electrically driven intensity modulator to obtain weak Stokes and anti-Stokes sidebands. The three waves are then injected into the waveguide, where they couple via optomechanical interactions when the modulation frequency Ω sweeps across the Brillouin resonance. A reference line is added at the output of the device by up-shifting the pump frequency by $\Delta = 40$ MHz with an acousto-optic modulator. Then, the Stokes and anti-Stokes intensity is measured by heterodyne detection as an RF beating note using a fast photodetector and a radio-frequency (RF) spectrum analyzer. The experimental configuration can be interpreted as a gain enhancement scenario, as two processes take place simultaneously: the energy transfer from the anti-Stokes line to the pump, and the energy transfer from the pump to the Stokes line. In the following, Brillouin gain or loss will be used to refer to the relative change in intensity for Stokes and anti-Stokes lines, although it should be kept in mind the different pumping schema with respect to the traditional Brillouin experiment. All experimental measurements were taken under laboratory conditions, i.e., at room temperature and ambient pressure.

In **Figure 4a**, we illustrate the normalized Stokes and anti-Stokes intensity as a function of the modulating frequency for different input pump powers. In all the cases, the input powers for Stokes and anti-Stokes probes were 15 dB lower. The waveguide under study has a length of 6 mm, with 6.5 dB cm^{-1} of linear loss and we input and output light from it using grating couplers with an efficiency of 16%. The anti-Stokes line experiences a depletion, while the intensity of the Stokes line increases, both resulting from the energy transfer mediated by the Brillouin effect. These spectra show a Lorentzian shape centered at the frequency of the mechanical mode that mediated the coupling, also known as the Brillouin shift. By fitting the experimental data to the nonlinear theoretical model, we can retrieve the main parameters that characterize the interaction. Hence, we obtain a mechanical frequency of $\nu_m = \Omega_m/2\pi = 7.0452 \pm 0.0001$ GHz, a linewidth of $\gamma_m = \Gamma_m/2\pi = 6.4 \pm 0.5$ MHz for the optomechanical interaction ($Q_m = \nu_m/\gamma_m \approx 1050$), and a Brillouin coefficient of $G_B = 1361 \pm 44 \text{ W}^{-1} \text{ m}^{-1}$. These values show a good agreement with the predicted ones ($\nu_m = 7.184$ GHz and $G_B = 2046$

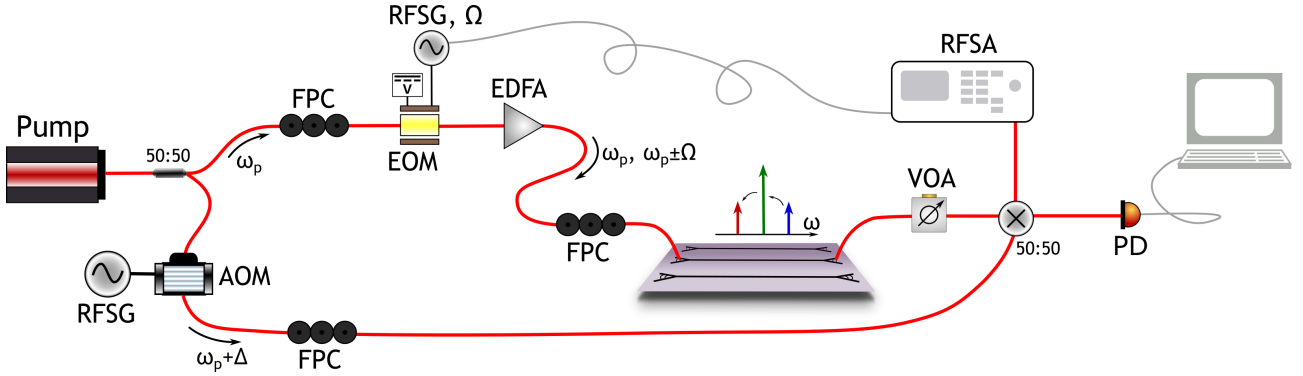


Figure 3: Experimental setup. Two processes of energy transfer take place in the waveguide: from the blue-detuned anti-Stokes sideband (ω_{as}) to the pump line (ω_p), and from the pump line to the red-detuned Stokes sideband (ω_s). A reference line with up-shifted frequency with respect to the pump ($\omega_p + \Delta$) is used to distinguish between both sidelines in the RF spectrum. AOM, acousto-optic modulator; EDFA, erbium-doped fiber amplifier; EOM, electro-optic modulator; FPC, fiber polarization controller; PD, photodetector; RFSA, RF spectrum analyzer; RFSG, RF signal generator; VOA, variable optical attenuator.

$W^{-1} m^{-1}$) albeit some deviations resulting from differences in the material parameters between the fabricated and simulated waveguide and fabrication errors and inhomogeneities.

The power dependency of the Brillouin gain and loss is also in good accordance with the theoretical model, as shown in Figure 4b and 4c for two different waveguide lengths: 6 mm (b) and 4 mm (c). Brillouin interaction is a cumulative effect, and so, the longer the waveguide, the larger the Brillouin gain or loss. It should be mentioned here the Brillouin parameters obtained for the 4 mm-long waveguide by fitting the corresponding RF spectra, which are $\nu_m = 7.0426 \pm 0.0002$ GHz, $\gamma_m = \Gamma_m/2\pi = 7.6 \pm 0.8$ MHz, and a Brillouin coefficient of $G_B = 970 \pm 42$ $W^{-1} m^{-1}$. Additionally, we observe an asymmetry between the gain in the Stokes signal and the depletion of the anti-Stokes in the longest waveguide, barely noticeable in the shortest one. Thus, for the 6mm-long waveguide, a maximum of 1.9 dB of depletion is achieved with 35.5 mW input power for the anti-Stokes sideband, while a maximum of 1.4 dB of gain is achieved for the Stokes line with the same input power. Despite the strong optomechanical interaction this waveguide yields, the moderately high linear losses due to surface roughness prevent reaching the net gain regime. Enlarging the waveguide width, often seen in literature as a way to reduce this issue, would worsen also the Brillouin coupling, as the overlap between acoustic and optical mode profiles will be lower. Hence, the reduction of surface roughness should rely on improved fabrication processes. Nevertheless, the results presented in this paper can be sufficient to create narrow-linewidth notch filters [19, 20]. Additionally, the extended profile of the mechanical mode in our waveguides may lead to highly nonlocal nonlinearities [21] that can be used to couple different optical waveguides to provide a coherent control of information [22] or shape and RF signal [23].

Finally, we study the possibility of tuning the mechanical response of our geometry. As mentioned before, FBS couples transversally propagating phonons and longitudinally propagating photons. Therefore, variations of the geometry perpendicular to the waveguide axis allow us to tailor the acoustic mode without affecting the optical one. By playing with different waveguide and subwavelength arm widths (W_c and W_{swg} in Figure 1) we can obtain a collection of mechanical resonances localized in the bandgap of the phononic crystal (Figure 2a) to ensure good confinement. In **Figure 5**, we present the normalized RF spectra for the

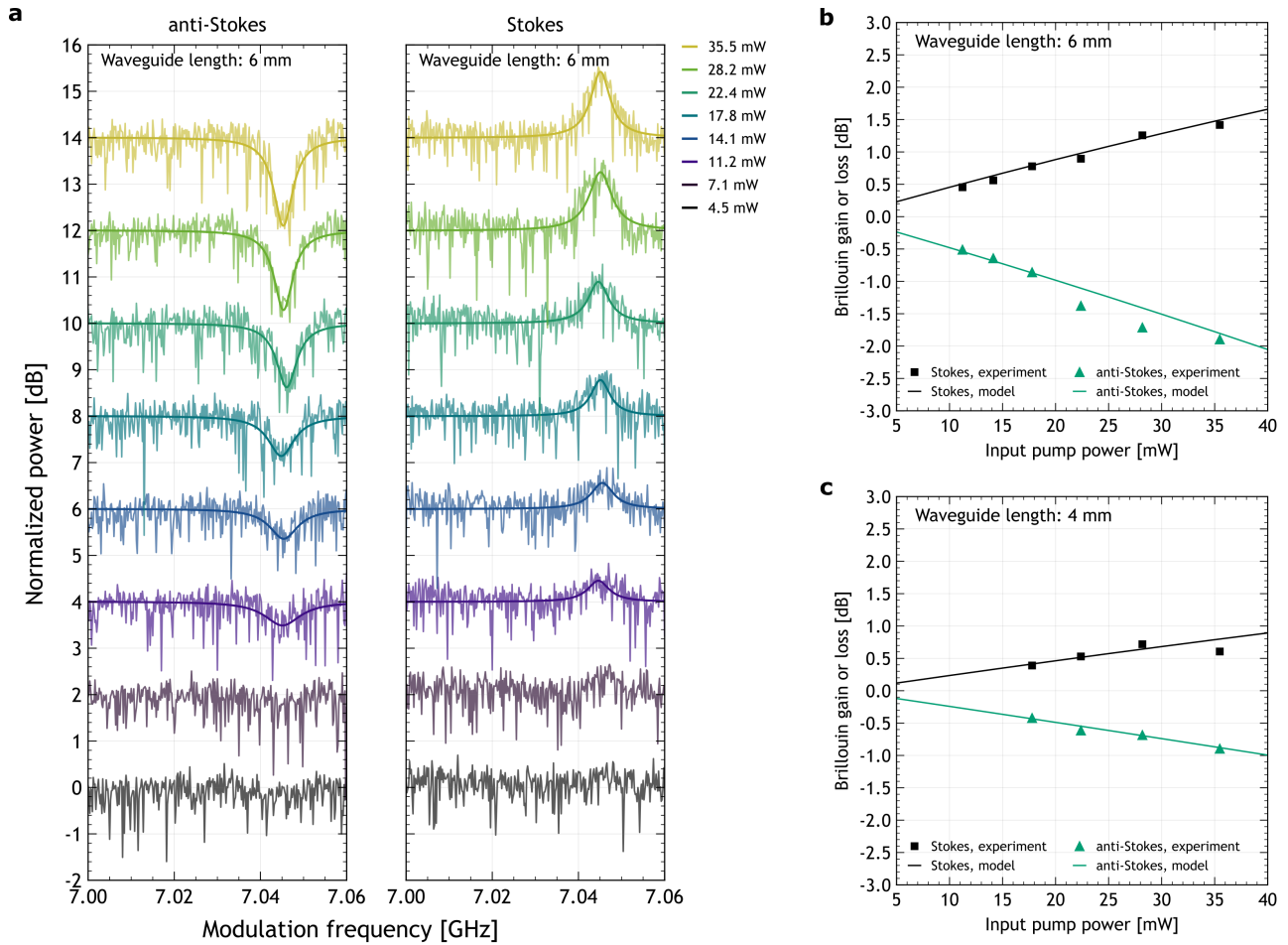


Figure 4: Brillouin gain and loss in the proposed optomechanical waveguide. a) RF beat note between pump and Stokes or anti-Stokes lines as a function of the modulating frequency for different input pump powers. b) and c) Brillouin gain (black) and loss (green) of the Stokes and anti-Stokes, respectively, for two different waveguide lengths. Here, squares and triangles represent the experimental measurements, while the solid lines stand for the theoretical model.

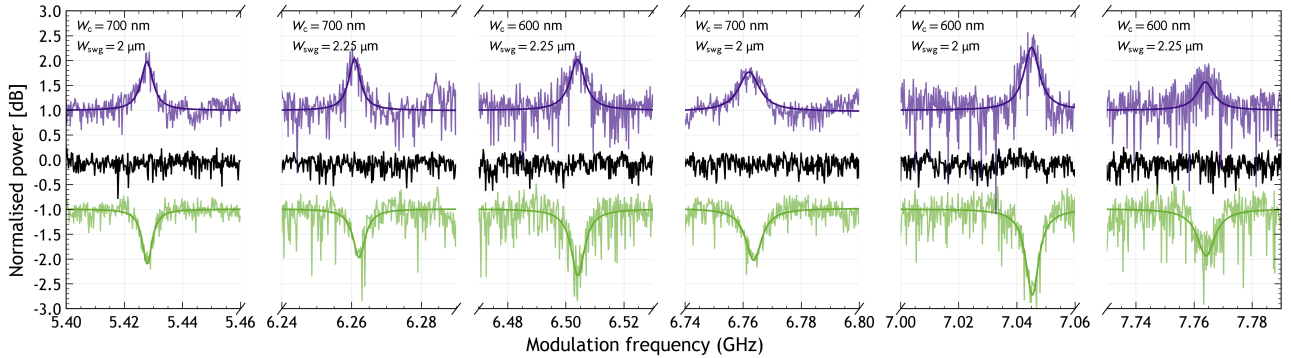


Figure 5: Normalized RF spectra for the Stokes (purple) and anti-Stokes (green) sidebands for different transversal geometries of our waveguide and an input pump power of 28 mW. In black, we plot the RF beating note of the anti-Stokes line for a reference waveguide. All measured waveguides were 6 mm long.

Table 1: Characteristic Brillouin parameters for different geometries. Here, ν_m refers to the mechanical frequency, γ_m to the optomechanical interaction linewidth, and G_B to the Brillouin coefficient. In all cases, the measured waveguide has a length of 6 mm.

Geometry	ν_m [GHz]	γ_m [MHz]	Q_m	G_B [$W^{-1} m^{-1}$]
$W_c = 700$ nm, $W_{swg} = 2.00$ μm	5.4278 ± 0.0002	4.9 ± 0.3	1108	1254 ± 52
$W_c = 700$ nm, $W_{swg} = 2.25$ μm	6.2611 ± 0.0003	4.8 ± 0.3	1304	1050 ± 57
$W_c = 600$ nm, $W_{swg} = 2.25$ μm	6.5044 ± 0.0001	7.9 ± 0.4	823	1317 ± 53
$W_c = 700$ nm, $W_{swg} = 2.00$ μm	6.7630 ± 0.0001	7.6 ± 0.5	902	984 ± 51
$W_c = 600$ nm, $W_{swg} = 2.00$ μm	7.0452 ± 0.0001	6.4 ± 0.5	1050	1361 ± 44
$W_c = 600$ nm, $W_{swg} = 2.25$ μm	7.7638 ± 0.0002	7.6 ± 0.4	1022	970 ± 73

Stokes and anti-Stokes lines for different geometries. In all the cases, the waveguides are 6 mm long and the input pump power is around 28 mW. As before, the input power for the Stokes and anti-Stokes lines is 15 dB lower. We show that it is possible to tune the acoustic resonance in the range between 5 and 8 GHz (**Table 1**). Besides, the coupling efficiency, expressed by the Brillouin coefficient G_B remains elevated in all cases. For all the acoustic modes, the Brillouin parameters obtained upon fitting the experimental data to the theoretical model show good agreement with the simulated values. Hence, our waveguide provides comparable Brillouin interaction and mechanical confinement to similar structures in literature [10, 11, 18] using a single etching step, all-silicon waveguide. Nevertheless, as highlighted before, further improvement in optical propagation loss is needed to increase the Stokes gain and reach the net amplification regime.

4 Discussion and conclusion

We propose and demonstrate a new design for an optomechanical waveguide that yields a large Brillouin interaction. This geometry relies on a phononic crystal to confine the mechanical modes within the core and a subwavelength intermediate cladding to ensure optical propagation to moderate losses and provide mechanical stability. This design requires a single etching step, simplifying the fabrication process. We show a state-of-the-art optomechanical coupling, with an experimental value of G_B up to $1360 W^{-1} m^{-1}$, and a measured Stokes gain of 1.5 dB and

anti-Stokes depletion of -2 dB in a 6 mm-long waveguide and 35 mW of input power. Besides, our design allows for easy tailoring of the mechanical frequency within the range between 5 and 8 GHz and comparable performance by simple geometry modifications. These results open interesting perspectives for the implementation of narrow linewidth RF notch filters or the study of nonlocal nonlinearities in optical systems. A net Brillouin gain may be achieved by further reducing optical propagation losses, such as through post-processing to reduce sidewall roughness.

Acknowledgements

The fabrication was performed with the C2N micro nanotechnologies platforms and partly supported by the RENATECH network and the General Council of Essonne. This work has been funded by ANR BRIGHT (ANR-18-CE24-0023-01), the European Union (ERC-SPRING, under the Grant Agreement 101087901), and European Union's Horizon Europe (Marie Skłodowska-Curie grant agreement N^o 101062518). Views and opinions expressed are, however, those of the author(s) only and do not necessarily reflect those of the European Union or the European Research Council. Neither the European Union nor the granting authority can be held responsible for them.

References

- [1] S. Gundavarapu, G. Brodnik, M. Puckett, T. Huffman, D. Bose, R. Behunin, J. Wu, T. Qiu, C. Pinho, N. Chauhan, J. Nohava, P. Rakich, K. Nelson, M. Salit, D. Blumenthal, *Nature Photonics* **2019**, *13*, 1 60.
- [2] M. Merklein, B. Stiller, I. V. Kabakova, U. S. Mutugala, K. Vu, S. J. Madden, B. J. Eggleton, R. Slavík, *Opt. Lett.* **2016**, *41*, 20 4633.
- [3] E. A. Kittlaus, P. Kharel, N. T. Otterstrom, Z. Wang, P. T. Rakich, *Journal of Lightwave Technology* **2018**, *36*, 13 2803.
- [4] J. B. Murray, A. Cerjan, B. Redding, *Optica* **2022**, *9*, 1 80.
- [5] M. Merklein, B. Stiller, K. Vu, P. Ma, S. J. Madden, B. J. Eggleton, *Nanophotonics* **2021**, *10*, 1 75.
- [6] J. Zhang, C. Zhu, C. Wolff, B. Stiller, *Phys. Rev. Res.* **2023**, *5* 013010.
- [7] A. Kobayakov, M. Sauer, D. Chowdhury, *Adv. Opt. Photon.* **2010**, *2*, 1 1.
- [8] Peter T. Rakich, Charles Reinke, Ryan Camacho, Paul Davids, Zheng Wang, *Physical Review X* **2012**, *2*, 1 011008.
- [9] G. S. Wiederhecker, P. Dainese, T. P. Mayer Alegre, *APL Photonics* **2019**, *4*, 7 071101.
- [10] H. Shin, W. Qiu, R. Jarecki, J. A. Cox, R. H. Olsson, A. Starbuck, Z. Wang, P. T. Rakich, *Nature Communications* **2013**, *4*, 1 1944.
- [11] E. A. Kittlaus, H. Shin, P. T. Rakich, *Nature Photonics* **2016**, *10*, 7 463.

- [12] R. V. Laer, A. Bazin, B. Kuyken, R. Baets, D. V. Thourhout, *New Journal of Physics* **2015**, *17*, 11 115005.
- [13] R. Van Laer, B. Kuyken, D. Van Thourhout, R. Baets, *Nature Photonics* **2015**, *9*, 3 199.
- [14] R. Halir, P. J. Bock, P. Cheben, A. Ortega-Moñux, C. Alonso-Ramos, J. H. Schmid, J. Lapointe, D.-X. Xu, J. G. Wangüemert-Pérez, Í. Molina-Fernández, S. Janz, *Laser & Photonics Reviews* **2015**, *9*, 1 25.
- [15] Y.-F. Wang, Y.-S. Wang, *Journal of Sound and Vibration* **2013**, *332*, 8 2019.
- [16] C. Wolff, B. Stiller, B. J. Eggleton, M. J. Steel, C. G. Poulton, *New Journal of Physics* **2017**, *19*, 2 023021.
- [17] P. Kharel, R. O. Behunin, W. H. Renninger, P. T. Rakich, *Phys. Rev. A* **2016**, *93* 063806.
- [18] K. Wang, M. Cheng, H. Shi, L. Yu, C. Huang, S. Qin, Y. Zhang, L. Kai, J. Sun, *ACS Photonics* **2021**, *8*, 9 2755.
- [19] A. Casas-Bedoya, B. Morrison, M. Pagani, D. Marpaung, B. J. Eggleton, *Opt. Lett.* **2015**, *40*, 17 4154.
- [20] Y. Liu, A. Choudhary, G. Ren, K. Vu, B. Morrison, A. Casas-Bedoya, T. G. Nguyen, D.-Y. Choi, P. Ma, A. Mitchell, S. J. Madden, D. Marpaung, B. J. Eggleton, *APL Photonics* **2019**, *4*, 10 106103.
- [21] S. Gertler, P. Kharel, E. A. Kittlaus, N. T. Otterstrom, P. T. Rakich, *New Journal of Physics* **2020**, *22*, 4 043017.
- [22] H. Kim, H. Shin, *Nano Letters* **2021**, *21*, 17 7270.
- [23] H. Kim, Y. Seong, K. Kwon, W. Shin, S. Lee, H. Shin, *ACS Photonics* **2022**, *9*, 9 2938.